

Ro-Vibrational Spectroscopy in Hybrid fs/ps-CARS for N₂ Thermometry

M. Nafa
(ONERA/Institut UTINAM,
UMR CNRS 6213)

M. Scherman,
A. Bresson, A. Aubin, A. Godard,
B. Attal-Tretout
(ONERA)

P. Joubert
(Institut UTINAM, UMR CNRS 6213)

E-mail: michael.scherman@onera.fr

DOI : 10.12762/2016.AL12-10

Ro-vibrational CARS spectroscopy is performed on the Q-branch of N₂ in the hybrid fs/ps regime. A new optical setup has been mounted using a single laser source and a spectral filtering stage based on a volume Bragg grating and a Fabry-Perot etalon, in order to achieve a good enough resolution. CARS spectra are recorded in ambient air at a 1 kHz repetition rate. However, a CH₄/air flame is probed at 2 Hz, in order to obtain a strong enough signal to enable thermometry. The theoretical treatment is also detailed and provides the calculated spectrum, properly compared to experimental profiles in order to retrieve the temperature. The accuracy of the hybrid fs/ps-CARS thermometry is satisfactory as regards the state of the art, but further experiments are in progress to increase the repetition rate of the measurement in hot gases.

Introduction, Context

CARS spectroscopy for diagnostics in reactive flows

Laser techniques have high spatial and temporal resolution, enabling locally and temporally resolved measurements of temperature and species concentration. Among the various optical diagnostics, non-linear techniques provide stronger and collimated signals allowing highly luminous media at high temperature and pressure to be studied *in situ* [1]. One of them, coherent anti-Stokes Raman scattering (CARS), was developed at ONERA [2] and extensively used for temperature measurements in hostile reactive environments of interest in the aeronautic field [3] [4].

CARS is a nonlinear spectroscopic technique that was first introduced by Maker *et al.* [5]. As illustrated in Figure 1 (a), a CARS process takes place when three laser beams, namely pump, Stokes and probe, propagate through a medium having Raman active ro-vibrational modes $\omega_{\alpha\beta}$, described by the vibration and rotation quantum numbers ν and J of the ro-vibrational levels $|\alpha\rangle$ and $|\beta\rangle$ associated with the transition. When pump and Stokes fulfill $\omega_p - \omega_s = \omega_{\alpha\beta}$, a new wave is generated at the anti-Stokes frequency $\omega_{AS} = \omega_{pr} + \omega_{\alpha\beta}$. It results from the inelastic scattering of the wave ω_{pr} by the molecular vibrations, coherently driven by the

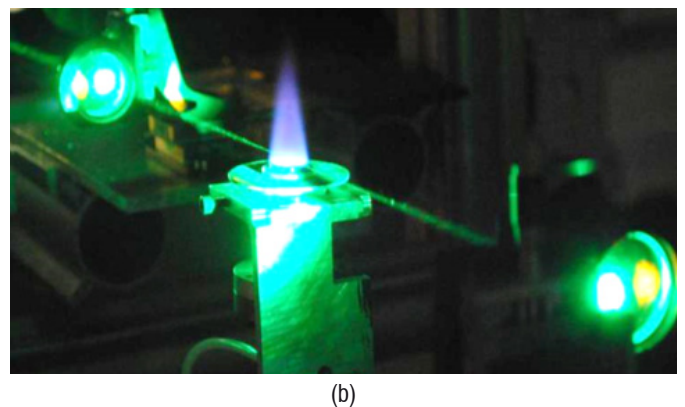
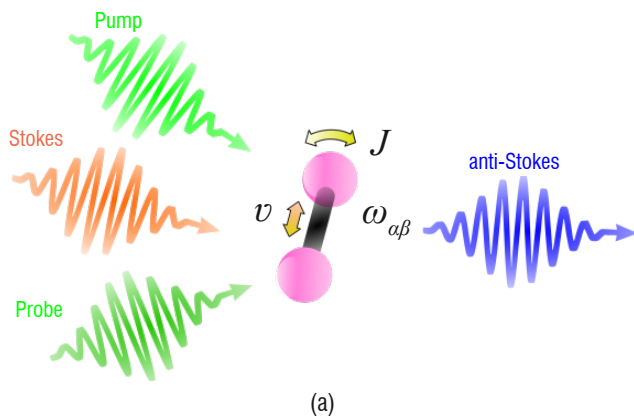


Figure 1 – (a) Sketch of the CARS process: generation of an anti-Stokes signal by a N₂ molecule, with rotational and vibrational degree of freedom designated by their respective quantum number J and ν , excited by three laser pulses, pump, Stokes and probe. (b) Illustration of CARS diagnostics in a CH₄/air flame.

incident waves at ω_p and ω_s . By scanning the Stokes wavelength, the molecular spectrum can be obtained [6], while a broadband pulse allows it to be recorded in a single laser shot [7].

Over the last three decades, ns and ps-CARS spectroscopy appeared to be very well suited to gas phase diagnostics, such as temperature and concentration measurements in flames, as illustrated in Figure 1 (b). CARS diagnostics were used in this regime at a repetition rate of a few Hz, although 100 kHz CARS thermometry was recently demonstrated with ps-pulses using burst pulse lasers [8]. However, over the last ten years, the development of femtosecond lasers enabled to take advantage of good stability from shot to shot to increase the measurement accuracy, as well as high peak power to enhance the CARS process efficiency and allowing high repetition rate measurements [9]. Also, laser pulses benefit from large bandwidths, which were used to excite and probe wide spectral ranges in a single shot [10] [11] [12], thereby providing the broadband spectroscopy demonstrated previously [7] [13].

However, although gas spectroscopy was straightforward in the nanosecond or picosecond regime, a good enough spectral resolution was not easily achieved in the fs-regime due to the large bandwidth involved in the interaction. Moreover, the stationary approximation is no longer valid when the state lifetime becomes larger than the laser pulse duration and transient solutions of the system evolution thus need to be calculated [14]. Recently, a mixed regime called hybrid fs/ps, has been proposed to take advantage of both the broadband spectral range excited by fs-pulses, and the good resolution provided by ps-pulses [15]. It opens new possibilities for CARS diagnostics, and was successfully used to demonstrate single-shot pure-rotational [16] and under-resolved ro-vibrational [17] thermometry, ultra-broadband kHz punctual and 1D-CARS spectroscopy [18], and finally 10 Hz 2D-thermometry using pure rotational CARS [19]. In that context, our paper is aimed at investigating some specific properties of ro-vibrational CARS spectroscopy in the hybrid fs/ps regime and its potential application to thermometry.

Hybrid fs/ps-CARS spectroscopy for thermometry

The basic principle of temperature measurements by CARS is to probe the relative population of the molecular levels from which the thermodynamic temperature of the molecular system is drawn. The temperature is derived from the observed Q-branch ($\Delta J=0$, $\Delta v=+1$) of the N_2 CARS spectrum, as illustrated in Figure 2 (a), which is fitted to a library of theoretical shapes simulated assuming temperatures, potentially distinct, for vibration and rotation of N_2 molecules [20]. This technique is appropriate for diagnostics in non-equilibrium or very luminous reactive flows, such as plasma and flames, since the CARS process efficiency is high and the Raman shift of N_2 is well separated from those of other chemical species.

Hybrid fs/ps-CARS is described as a pump/probe experiment, and is illustrated in Figure 2. First, the medium is excited by ultra-short pump and Stokes fs-pulses that allow efficient broadband excitation of a set of Raman coherences, depicted in Figure 2 (b). Then, a narrowband ps-probe pulse interrogates the medium during a time that drives the final resolution on the anti-Stokes spectrum, as described in Figure 2 (c). Also, the excitation is separated from the probing of the coherences when using a pump/probe delay τ , which represents a new degree of freedom, compared to ns-CARS, to improve CARS performances, as illustrated in Figure 2 (d). As a result, non-resonant background rejection, which was a main limitation of ns-CARS, is optimized using τ [21] [22], thanks to the long-lived coherences induced from short pulse excitation. The timescale of the process has been well described by time diagrams in [1]. Moreover, as will be described later, in that particular time scale of photon interactions, the final anti-Stokes spectrum is shaped by both the molecular spectral signature and the temporal dephasing between rotational lines. It was used to drive the interferences and improve the diagnostic performances [23], [24], or to perform time-domain spectroscopy [15].

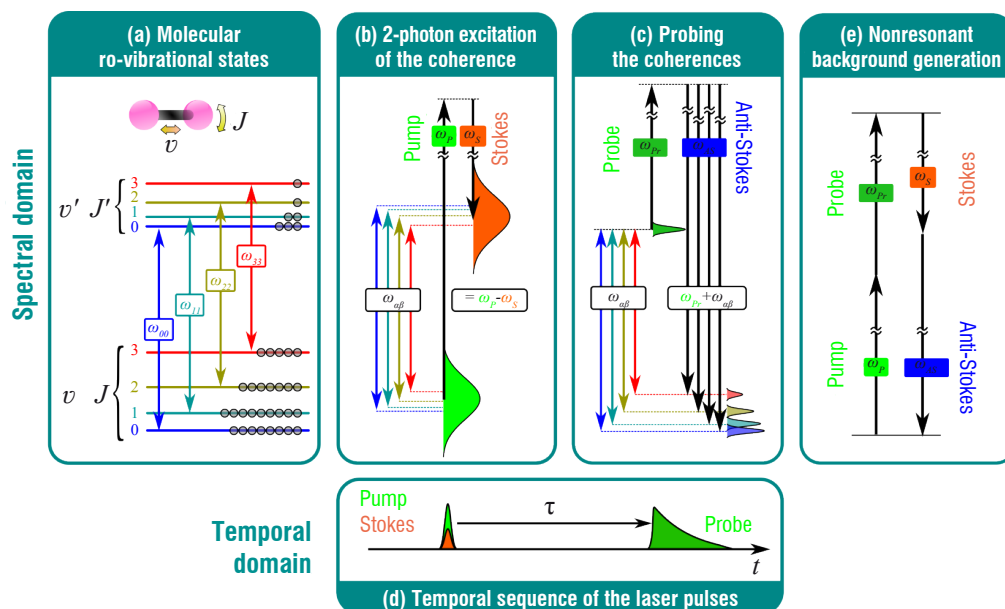


Figure 2 – Sketch of the light-matter interaction in hybrid fs/ps-CARS. (a) Energy level diagram of the N_2 rotational (J) and vibrational (v) structure, and Q-branch associated Raman transitions $\omega_{\alpha\beta}$. (b) Broadband excitation of the molecular coherences using a femtosecond pump and Stokes pulses at the respective frequencies ω_p and ω_s . (c) Narrowband probing using a picosecond probe pulse at frequency ω_{pr} and generating a well resolved anti-Stokes spectrum at $\omega_{AS} = \omega_{pr} + \omega_{\alpha\beta}$. (d) Temporal sequence of the laser pulses, in which pump and Stokes overlap and τ is the pump/probe delay. (e) Two-photon absorption (TPA) scheme contributing to CARS signal.

Experimental setup

General description of the experiment

The experimental setup is sketched in Figure 3. The laser beams generation stage, which is illustrated in Figure 3 (a), is based on a single industrial Yb:KGW laser (LightConversion) that delivers 150 fs – 1 mJ pulses at a 1 kHz repetition rate. A commercial optical parametric amplifier (OPA) with a second harmonic converter (LightConversion) is used to generate the tunable Stokes wavelength. It produces a 150 fs broadband (114 cm^{-1}) pulse of $21 \mu\text{J}$ energy at the Stokes wavelength of 583.5 nm. A leakage from the OPA pump, at 515 nm, is used to produce both the broadband (130 cm^{-1}) pump pulse of $60 \mu\text{J}$ energy, and the picosecond probe pulse. The latter is obtained by spectral filtering using a Fabry-Perot Etalon (FPE) and a volume Bragg grating (VBG, Optigrate). The narrowband pulse (0.7 cm^{-1}) is used as the CARS probe with about $1 \mu\text{J}$ energy. Residual spectral parasites are filtered out using high rejection filters (Semrock). The delay between the various pulses is controlled by two motorized translation stages. Recombination of the beams and focalization in a planar folded-BOXCARS geometry [25] are achieved using a dichroic mirror and a 300 mm focal length lens as shown in Figure 3 (b). The anti-Stokes signal is collected using a lens and a collection of interference filters (Semrock). It is then analyzed using a 750 mm spectrometer (Sopra) equipped with a 1800 line/mm grating, and coupled to an electron-multiplying CCD camera (Roper), as shown in Figure 3 (c). The flame was produced out of a McKenna burner, supplied by a CH_4/air mixture at an equivalent ratio $\phi=1$. The flat premixed flame is shown in Figure 1 (b).

Ps-probe spectral shaping

The temporal profile of the probe beam acts as a time-window to provide the molecular response. As a result, the probe bandwidth directly drives the resolution of the spectroscopy. Much effort has been devoted to precisely shape this spectral and temporal profile, as detailed in the following.

Various methods have been investigated by the hybrid fs/ps-CARS community, in order to generate the well suited picosecond pulse out of a femtosecond one. They are all aimed at narrowing the pulse bandwidth enough to resolve the fine structure of the spectrum, and to impose the right phase mask to generate an optimal temporal profile for the probe pulse. In particular, spatial light modulators [26] [27] [28], commercial filters [29], Fabry Perot etalons [30] [31], and non-linear bandwidth compressors [32] were implemented and tested in this double objective. They enabled the generation of pulses with few wavenumbers spectral width, and with asymmetrical temporal shape that proved to be optimal for CARS signal generation [33] [34]. In our case, the bandwidth condition is given by the spacing of the rotational lines, which is less than 1 cm^{-1} in N_2 , thus pushing the previously mentioned techniques to a challenging limit.

Monolithic devices are used in our case to shape both the amplitude and phase of the spectral profile. A volume Bragg grating (VBG) was used as a commercially available ultra-narrow amplitude filter [35]. The modulation of the refractive index, encoded in the thick transparent material, reflects a very thin part of the input spectrum that fulfills the Bragg condition. In our setup, a 10 mm thick VBG in photo-thermo-refractive (PTR) glass is used to generate a 0.7 cm^{-1} (FWHM) pulse, as shown in Figure 4 (a).

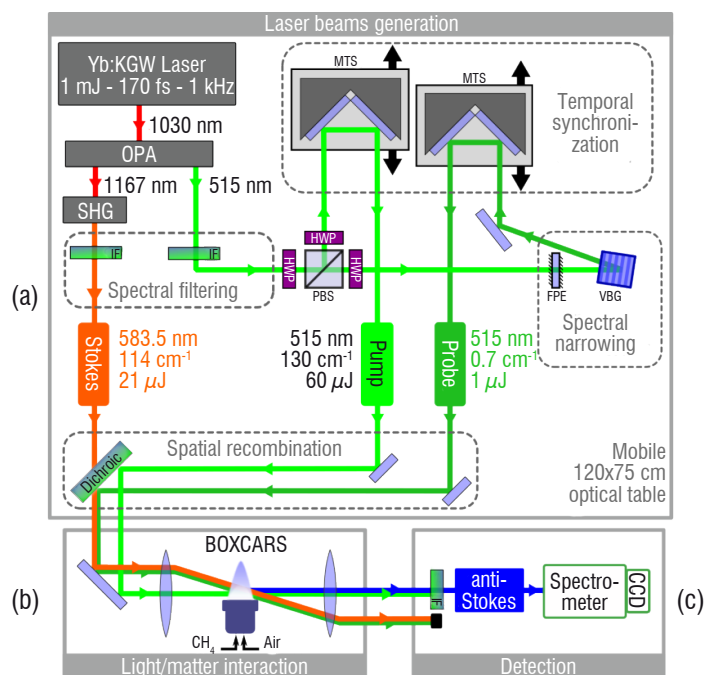


Figure 3 – Experimental setup: (a) laser beam generation, (b) light-matter interaction in the CH_4/air premixed flame with planar BOXCARS geometry, (c) anti-Stokes detection. OPA: Optical Parametric Amplifier, SHG: second harmonic generation, IF: interferential filter, PBS: polarizing beam splitter, HWP: half-wave plate, FPE: Fabry-Perot etalon, VBG: volume Bragg grating, MTS: motorized translation stage.

Phase shaping was achieved using a $100 \mu\text{m}$ thick FPE that was added upstream from the VBG, to reduce the energy and peak power delivered to the latter. The linewidth of the FPE frequency comb is 1.8 cm^{-1} , thus simplifying the superposition of the VBG reflection peak on the FPE transmission peak. The amplitude profile at the output of the filtering stage is thus fully driven by the VBG filter. However, the phase step that occurs at the FPE resonance peak is encoded into the spectrum of the pulse, and enables the generation of a time-asymmetric probe pulse, as plotted in Figure 4 (b). The temporal profile of the probe pulse was obtained by recording the CARS signal of pure Ar while scanning the pump-probe delay over an adequate range ($\sim 100 \text{ ps}$) [16]. In this case, the nonresonant CARS signal is proportional to the instantaneous superposition of the short pump/Stokes excitation ($\sim 150 \text{ fs}$ FWHM) with the long probe pulse ($\sim 30 \text{ ps}$ FWHM), thus providing a simple way to sample the temporal intensity profile of the probe (Figure 4(b)).

The Fourier Transform of the temporal profile has been calculated, assuming a flat temporal phase. The intensity (dotted line) and the phase (thick solid line) of the spectrum are plotted in Figure 4 (a). Good agreement between the calculated intensity profile and the experimental spectrum (thin solid line) is observed, validating the flat temporal phase assumption. Moreover, the phase step that characterizes asymmetric pulses generated by FPE could be evaluated. As a result, this set of commercial filters enabled a well suited probe profile to be shaped, *i.e.*, temporally asymmetric, and spectrally narrow enough to probe the rotational lines of N_2 , as will be seen later on.

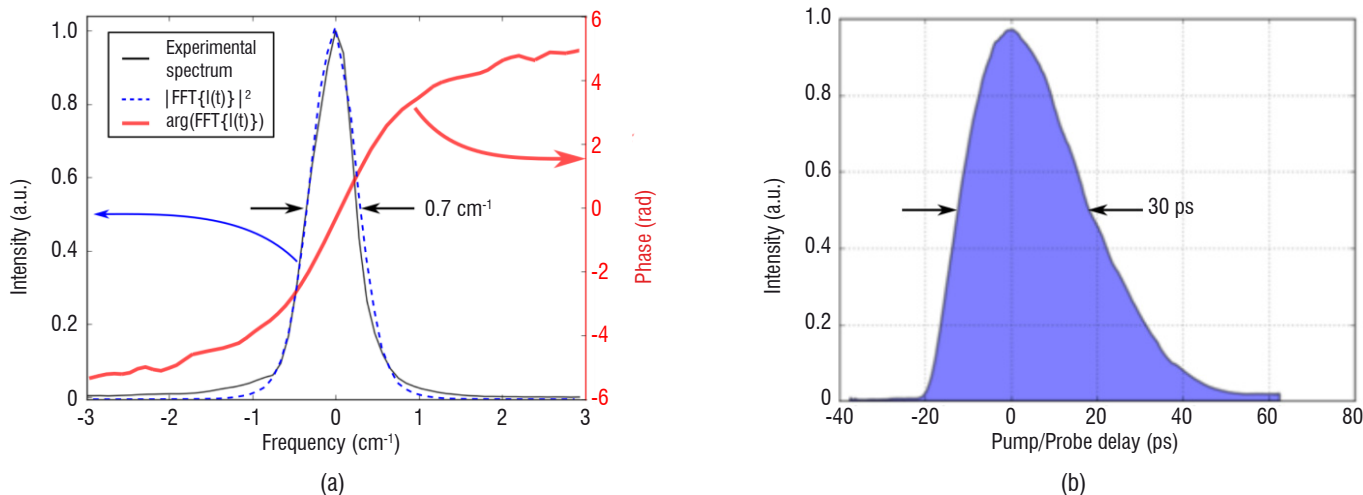


Figure 4 – (a) Spectral and (b) temporal characterization of the generated probe pulse through the filtering stage. (a) The experimental spectrum (thin solid line) is compared to the intensity (dotted line) and phase (thick solid line) of the Fourier transform of the temporal profile.

Characterization of the pump/Stokes excitation

The effective Raman bandwidth excited by the pump/Stokes pulses was measured by recording the nonresonant CARS signal in Ar. The spectral excitation profile ($\sim 100 \text{ cm}^{-1}$ FWHM) centered on the N_2 first vibrational band is shown in Figure 5. The amplitude distribution of the various ro-vibrational lines of N_2 at flame temperature ($\sim 2500 \text{ K}$) is shown in blue for comparison. The excitation bandwidth is thus well suited for N_2 spectroscopy in combustion, since the main intense vibrational bands, $\nu=0 \rightarrow \nu'=1$, $\nu=1 \rightarrow \nu'=2$ and $\nu=2 \rightarrow \nu'=3$, are included in the green excitation window in Figure 5.

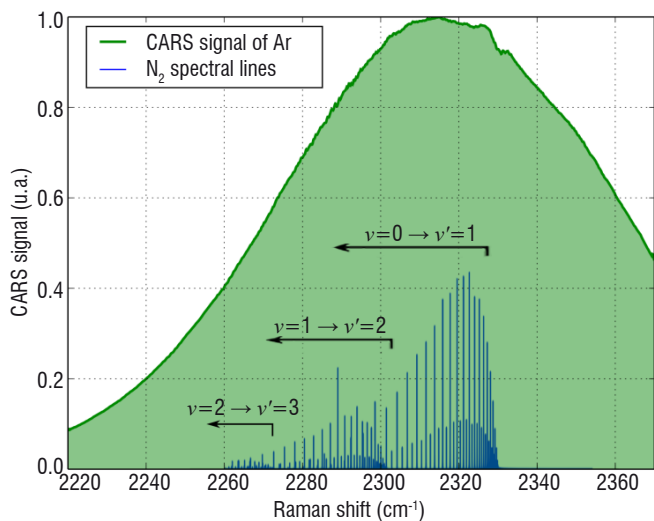


Figure 5 – Nonresonant CARS signal of Ar (green filled curve), illustrating the bandwidth effectively excited by pump and Stokes pulses, compared to the theoretical CARS spectrum of N_2 in a flame (blue lines).

This bandwidth is driven by the pump and Stokes spectral and temporal profiles. Indeed, while Fourier transform limited pump and Stokes pulses allow the excitation of a large spectral range, a chirp on one pulse, which delays the frequencies contained in the optical spectrum, may decrease the bandwidth, which is effectively excited, as illustrated in the spectrograms of Figure 6 (a). In our case, a commercial auto-correlator (Geco, LightConversion) is used to measure the pulse duration. The Stokes pulse proved to be Fourier transform limited, but a chirp was observed on the pump pulse. This aspect is investigated experimentally in Figure 6 (b), by monitoring the

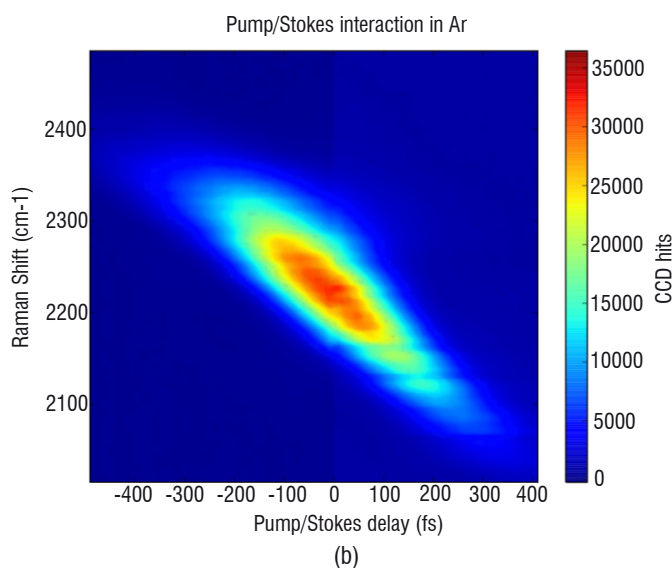
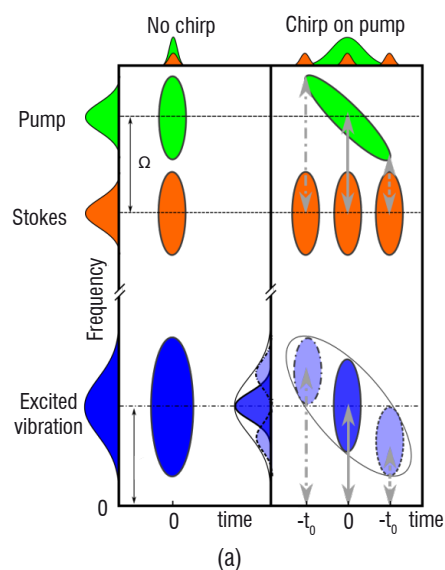


Figure 6 – Effect of a chirp on the CARS spectrum. (a) Illustration of the vibration range excited by a Fourier transform Stokes pulse and a Fourier transform (left), or chirped (right), pump pulse. (b) Experimental CARS spectrum (vertical) collected in Ar versus the pump/Stokes delay (horizontal).

location of the Ar CARS signal when the pump/Stokes delay is scanned. This effect was used in order to finely tune the excitation profile in the selected spectral range, by adjusting the pump/Stokes delay. In addition, it is important to quantify the chirp of the CARS excitation pulses in order to accurately simulate the CARS spectrum. Indeed, it may influence the temporal dephasing of the various excited coherences and thus the shape of the final spectrum, as will be seen later on. Finally, compensating techniques can be implemented to increase the excitation window.

N₂ spectroscopy

Ro-vibrational signature in the hybrid ps/fs regime

Resolving the ro-vibrational band structure

A major species of interest for thermometry is N₂. CARS spectra of N₂ were recorded in ambient air and in a CH₄/air flame, in order to evaluate the performances of the setup for thermometry. Figure 7 shows the experimental spectra recorded (a) in the ns-regime, which represents for us a typical reference spectrum, and (b) in the hybrid fs/ps-regime. An enlargement of the fundamental band of the Q-branch (2300-2335 cm⁻¹) is shown, to outline the rotational features provided by the two techniques. It appears that the two regimes allow both the vibrational and the rotational structures to be seen: three vibrational bands ($\nu = 0 \rightarrow \nu' = 1$, $\nu = 1 \rightarrow \nu' = 2$ and $\nu = 2 \rightarrow \nu' = 3$) can be distinguished in the hot spectra, each one being composed of well-resolved rotational

lines, with characteristic 1/4 alternation amplitude of the even/odd lines [36]. It is of major importance in the diagnostics of non-equilibrium media that the two population distributions, corresponding to vibrational and rotational temperatures, are able to be measured independently [20].

As in ns-CARS, the sensitivity of hybrid fs/ps-CARS to temperature can be appreciated by comparing the hot and cold spectra. In ambient air (in blue), the signal is restricted to a 15 cm⁻¹ spectral range centered on the first rotational lines of the fundamental band, whereas in the hot spectra (in red) rotational lines are distributed over three vibrational bands. The performance of hybrid fs/ps-CARS ro-vibrational thermometry is thus expected to be comparable to that obtained in ns-CARS, since a similar type of information can be retrieved from the spectra.

Coherent beating of the Raman lines

As mentioned before, one of the specificity of hybrid fs/ps-CARS over traditional ns-CARS is the ability to separate the process into two steps. We consider that the fast excitation of the ro-vibrational coherences through pump and Stokes pulses can be separated from the medium interrogation by the probe pulse in the second step. In the gas phase, introducing a delay τ between these two steps is allowed, since the lifetime of the coherences (\sim few 100 ps to few ns) is large compared to the duration of the probe pulse (30 ps) [22]. This allows some limitations of ns-CARS to be circumvented, such as nonresonant background interference [21], as well as enabling new measurement strategies to be found [23].

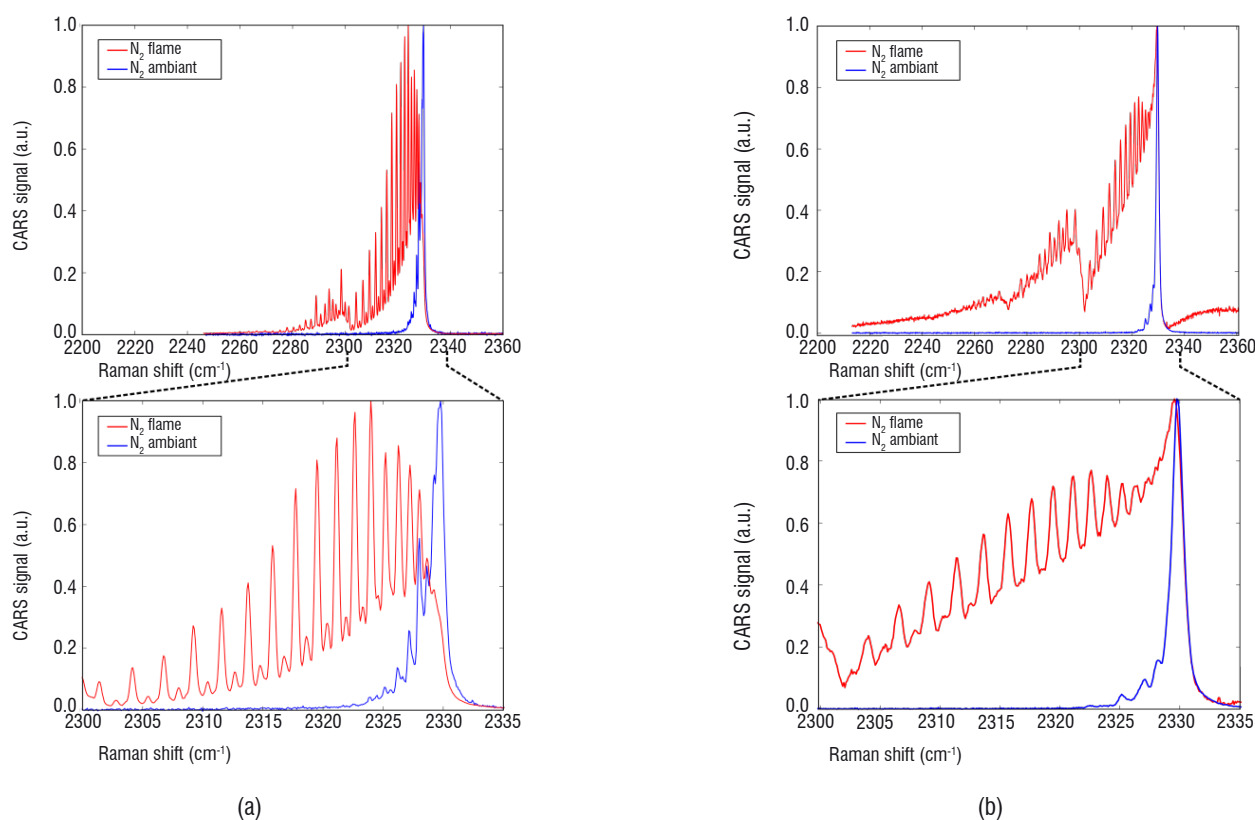


Figure 7 – Comparison of (a) ns-CARS and (b) the hybrid fs/ps-CARS spectra of the N₂ Q-branch obtained in ambient air (blue) and in flame (red). Bottom: enlargement of the fundamental vibrational band.

In Figure 8, the probe pulse delay is continuously scanned from -70 to 270 ps on the vertical axis using motorized delay lines. The CARS spectrum is monitored along the horizontal axis in ambient air, Figure 8 (a), and in the flame, Figure 8 (b). The zero delay position reported in the 2D plot is experimentally checked by maximizing the nonresonant signal. As previously observed in hybrid fs/ps CARS [15] [34] [23] [37] [31], periodic extinctions and revivals of the signal appear at positive delays, more particularly in Figure 8 (b), in which a broader range of ro-vibrational lines is populated by temperature.

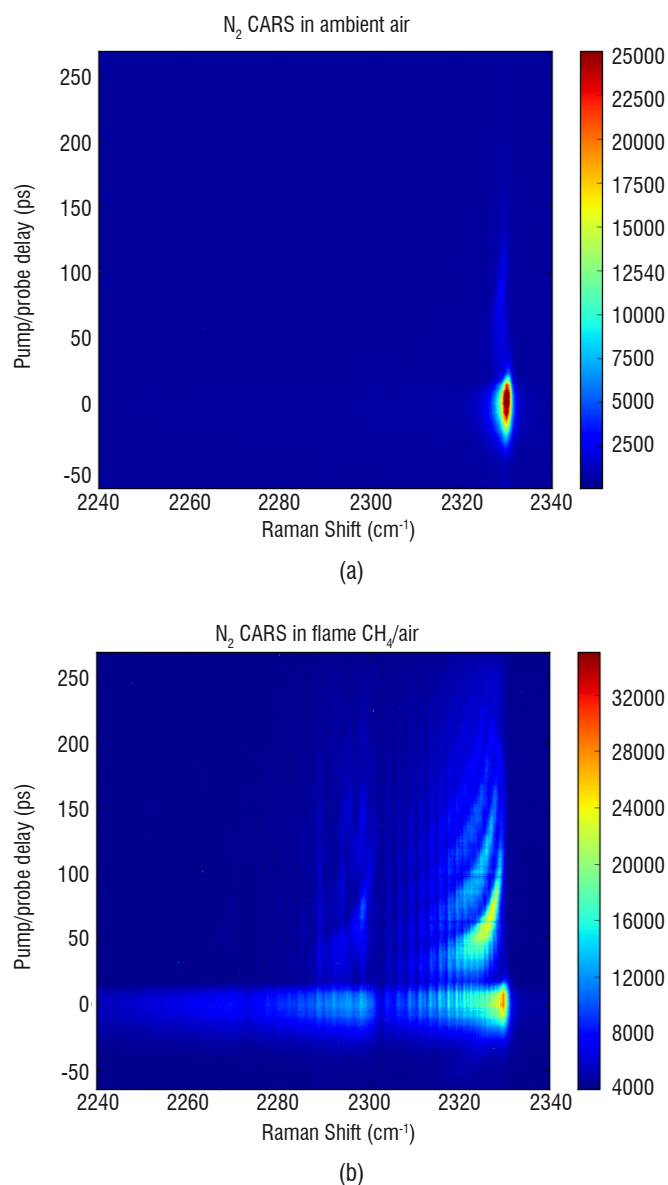


Figure 8 – Experimental investigation of the N_2 CARS spectrum (horizontal axis) evolution versus the pump/probe delay (vertical axis) (a) in ambient air, and (b) in a CH_4 /air flame.

In order to follow the modulation of individual Raman lines versus the pump/probe delay, an enlargement of the fundamental band is shown in Figure 9 (a). The evolution of the CARS amplitude at specific Raman shifts, corresponding to several rotational lines ($11 < J < 37$), is shown in Figure 9 (b). A rising edge is first observed at zero delay, when the probe coincides with the pump/Stokes excitation, which contains resonant and nonresonant contributions to the signal.

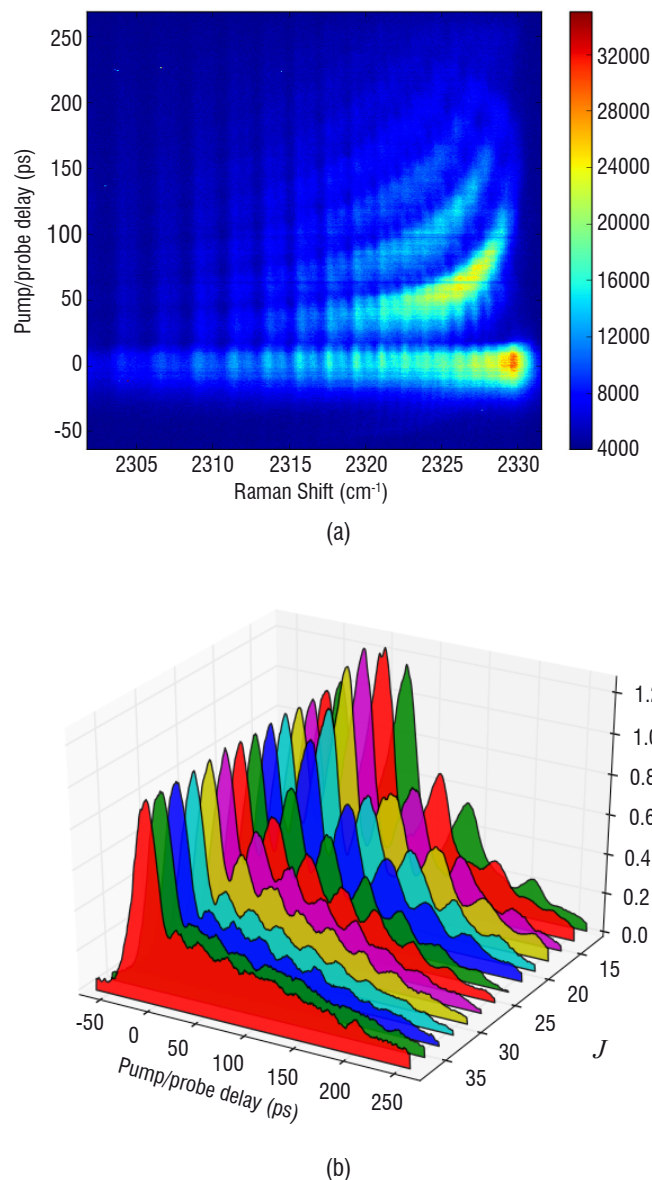


Figure 9 – (a) Evolution of the N_2 CARS spectrum (horizontal axis) centered on the fundamental vibrational band versus the pump/probe delay (vertical axis). (b) Evolution of the CARS intensity of the various rotational lines J of the fundamental vibrational band versus pump/probe delay.

As the probe delay increases, the nonresonant contribution disappears, and the resonant amplitude decays due to the finite lifetime of the coherences. Moreover, the CARS signal exhibits a sinusoidal pattern, whose amplitude and period decrease as a function of the quantum number J .

This behavior is attributed to interferences between rotational lines that occur in the hybrid fs/ps regime, as has already been observed by many authors [12] [37] [34] [23] [31] [38]. Indeed, as illustrated by Figure 10 (a), the multiples ro-vibrational coherences $\omega_{\alpha\beta}$ are excited simultaneously by pump and Stokes pulses. Then, during the free evolution that follows, the phase of each coherence evolves at its own frequency $\omega_{\alpha\beta}$, thus becoming dephased and rephased with respect to each other (Figure 10 (b)). Finally, during the interrogation step operated by the probe pulse, the contributions of the various lines may overlap, depending both on the line separation

and the probe linewidth. Consequently, they interfere constructively or destructively, depending on whether they are in or out of phase, and as a result the anti-Stokes intensity is modulated as plotted in Figure 10 (c).

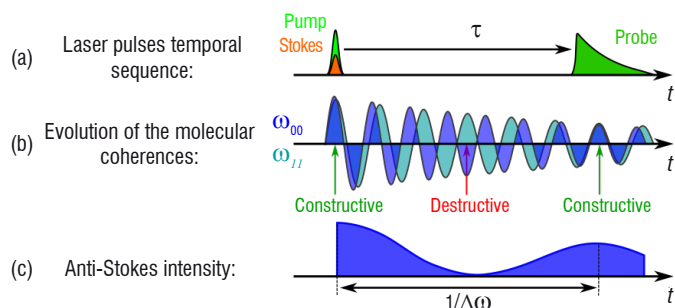
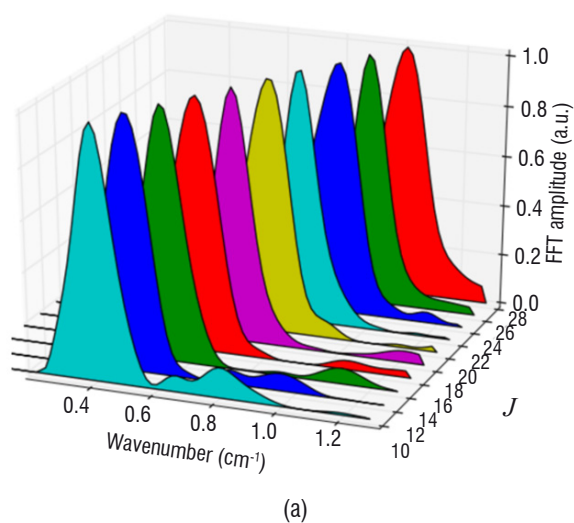


Figure 10 – (a) Typical laser sequence of the hybrid fs/ps-CARS process involving pump, Stokes and probe pulses. (b) Illustration of the dephasing and rephasing that occur between two ro-vibrational coherences, ω_{00} and ω_{11} , when the pump/probe delay τ evolves. (c) Effect of the dephasing on the anti-Stokes intensity when the contributions at ω_{00} and ω_{11} interfere: a modulation is observed with a period of $1/\Delta\omega$, where $\Delta\omega = |\omega_{00} - \omega_{11}|$.

In order to determine the modulation period, the Fourier Transform of the temporal evolution of the even Raman lines is processed in Figure 11 (a). For each J number, a main peak is observed at nonzero wavenumber, which corresponds to the modulation observed in the temporal domain. In Figure 11 (b), the peak spectral position is plotted as a function of the J value. It must be compared to the local spectral interval between rotational lines, which is calculated and also plotted along the vertical axis. It is given at first order in J by the expression:

$$\Delta\omega = 2\alpha_e (J + 1) \quad (1)$$

where α_e is the rotation-vibration coupling constant. The good agreement between calculations and experiment confirms the possibility of using the hybrid fs/ps regime to perform spectroscopy with a resolution better than the probe linewidth (0.7 cm^{-1}). Moreover, this interference pattern can be used as a spectral filter, in order to selectively attenuate or enhance specific spectral zones, as proposed by [23] [24].



Nonresonant background rejection

In the hybrid fs/ps regime, nonresonant background interference can be reduced by using a pump/probe delay [34], [33] [39] [28], as well as by crossing the polarizations of the pump, Stokes and probe beams, as has previously been done in ns-CARS spectroscopy [40] [41] [1]. CARS spectra in the CH_4/air flame have been recorded for three polarization configurations for the pump, Stokes and probe given in Figure 12 (a), (b) and (c). A Glan-polarizer is added upstream from the spectrometer to analyze the anti-Stokes signal.

The first configuration corresponds to parallel polarizations; the second one corresponds to the conventional technique of a 60° rotated Stokes [1] [42]; in the third one, the probe polarization is orthogonal to those of the pump and Stokes. In the three cases, the orientation of the anti-Stokes analyzer has been rotated every 10° , and CARS spectra have been acquired at each position, with 0° referring to the pump polarization direction. Typical spectra at the maximum and minimum CARS signal amplitude are shown in Figure 12 (a), (b) and (c). Because of a poor signal-to-noise ratio, due to the high degree of polarization of the anti-Stokes beam, the spectrum of Figure 12 (a) is given at 80° while extinction occurs at 90° , and the spectrum of Figure 12 (c) is given at 10° while extinction occurs at 0° . The amplitudes of the resonant (R) and nonresonant (NR) contributions are estimated using the CARS intensity at 2330 cm^{-1} and 2360 cm^{-1} respectively, and are shown in Figure 12 (d), (e) and (f). As expected, R and NR contributions appear respectively in phase and in quadrature for the parallel and the 60° rotated Stokes configuration schemes. This is illustrated in the CARS spectra, which show no distortion for the parallel case (Figure 12 (a)), and whose R and NR relative weight evolves in an opposite way to that of the 60° -Stokes (Figure 12 (b)), when the Glan analyzer is turned. It can be noticed that almost no NR contribution is observed in the 90° -crossed probe scheme and that the spectrum remains unaffected by nonresonant interference when the analyzer is crossed with respect to the probe. Indeed, CARS acquisitions in Ar with the parallel and the 90° -crossed probe configurations revealed that the latter permits the NR amplitude to be reduced by a factor of 8, while the resonant amplitude remained at similar level.

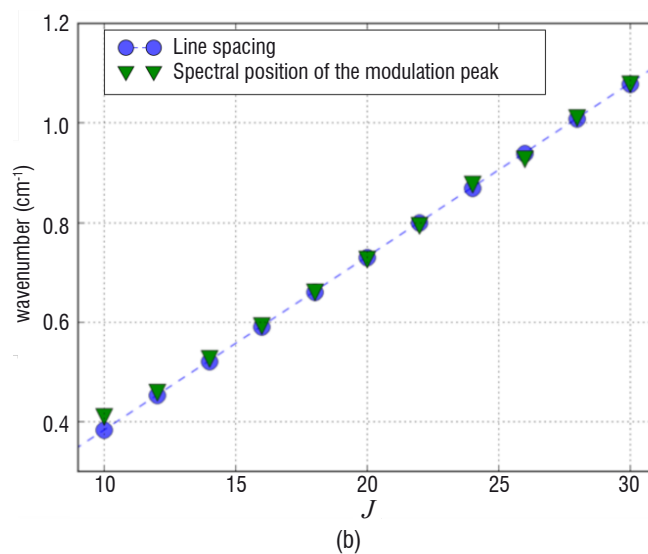
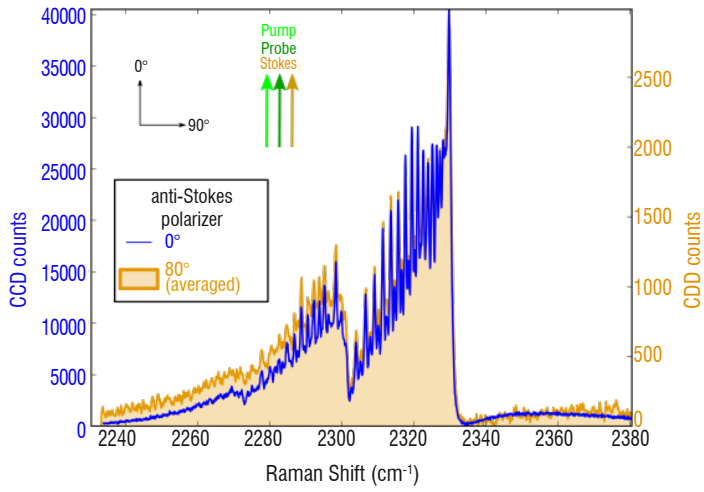
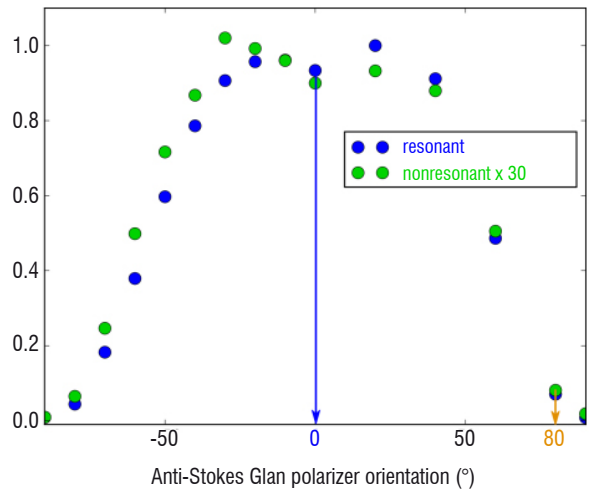


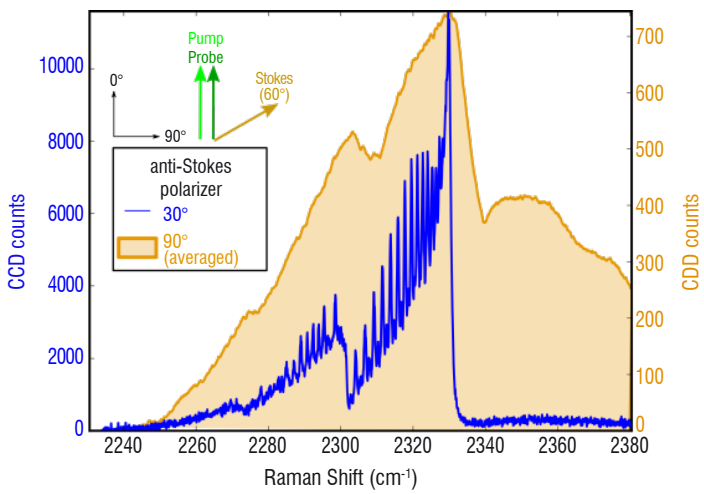
Figure 11 – Spectral analysis of the rotational line modulation on the first vibrational band. (a) Spectral modulation peak obtained by Fourier transform of the line CARS intensity temporal evolution as a function of the rotational quantum number J , and (b) comparison of the peak position (triangle) obtained experimentally with the local spectral interval between two successive Raman lines (circle), calculated using spectroscopic constants, as a function of J .



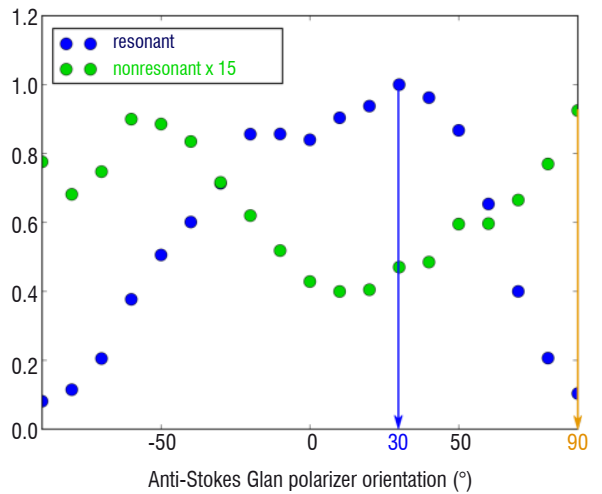
(a)



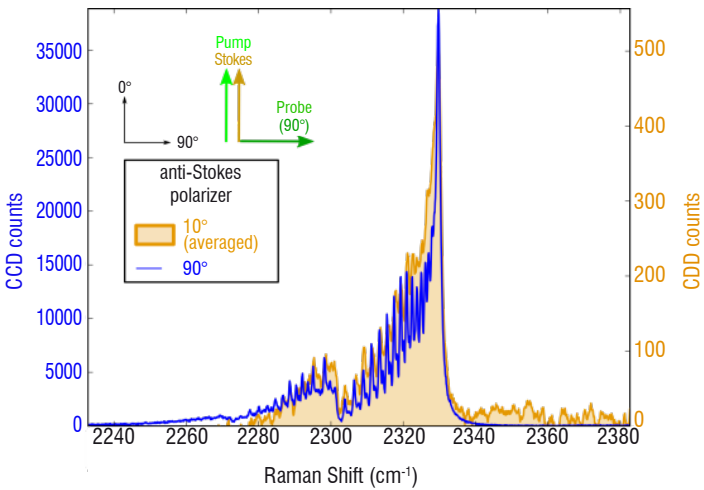
(d)



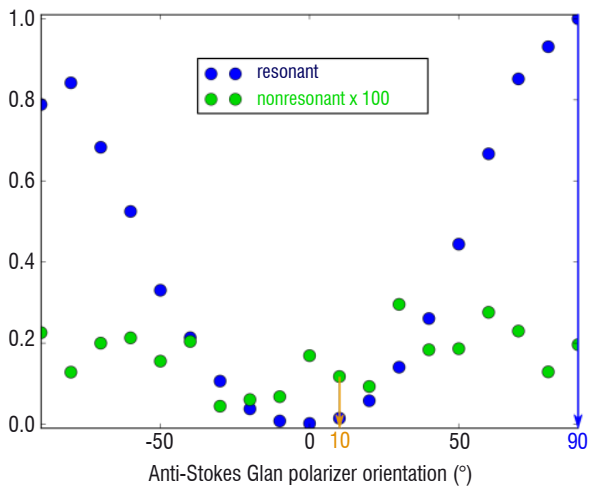
(b)



(e)



(c)



(f)

Figure 12 – N_2 CARS spectra at maximum and minimum signal amplitude obtained by rotating Glan-analyzer (a) parallel beams, (b) 60°-rotated Stokes, and (c) 90°-crossed probe. Resonant (blue circles) and nonresonant (green circles) contributions recorded for the 3 configurations are displayed in (d), (e) and (f).

2D plots of the CARS spectra of N_2 in a flame versus probe delay are shown in Figure 13 (a) for parallel polarizations, and in Figure 14 (a) for the crossed-probe configuration. At zero delay, a nonresonant contribution appears at the foot of the resonant line pattern only for parallel polarization. This can be seen in the spectra extracted from the dataset at 0 and 25 ps, shown in Figure 13 (b) and Figure 14 (b), in which the NR amplitude at 2360 cm^{-1} is always zero for the crossed-probe polarization. Moreover, the zero delay spectrum for the crossed polarization shows no distortion by NR contribution, while its shape at 25 ps is very similar to that obtained in the parallel configuration, since the signal is assumed to be purely resonant at this probe delay.

The crossed-probe configuration is observed to drastically attenuate the NR background, while the R signal is maintained. Attenuation is even stronger than expected from the conventional calculations [1], and thus attributed to the short pulse regime properties. Moreover, resonant contributions are maintained in this case, whereas a probe delay may lead to spectral distortions as a result of coherent line interferences. Indeed, polarization configuration, achieved using the 3 beam excitation of the hybrid regime, may provide a strong attenuation of the two photon

absorption (TPA) contributions to the CARS signal (Figure 2 (e)), thereby acting in favor of the R/NR ratio optimization. This should increase the measurement accuracy, since the temperature information is mainly enclosed in the resonant part, which is sensitive to the Boltzmann distribution. Moreover, a temperature estimation procedure should gain reliability, since the nonresonant contribution amplitude is usually left as a free parameter of the fit, or estimated from an assumption about the chemical composition of the medium, which introduces a bias in the measurement. Other polarization configurations will be studied in the future, in our laboratory.

Theoretical model and experimental spectra

Description of the model

We use a frequency-domain model equivalent to that reported by Stauffer *et al.* [37]. In the time-domain, the CARS amplitude is obtained by multiplying the probe pulse amplitude by the molecular response, convolved with the pump/Stokes excitation profile. We calculate the CARS amplitude as a function of the Raman shift

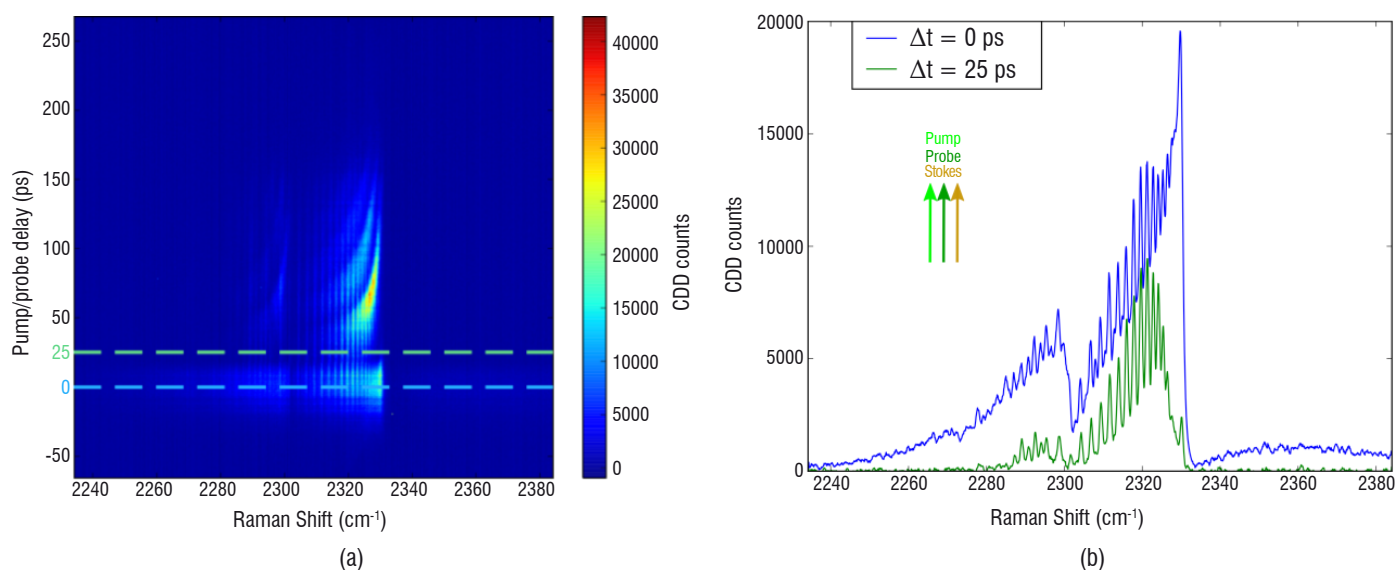


Figure 13 – N_2 CARS spectra recorded with vertical pump, Stokes and probe polarizations. (a) Evolution of the spectrum (horizontal axis) with the probe delay (vertical axis). The two dashed lines indicate the 0 and 25 ps delays. (b) Spectra recorded at the 0 and 25 ps probe delay

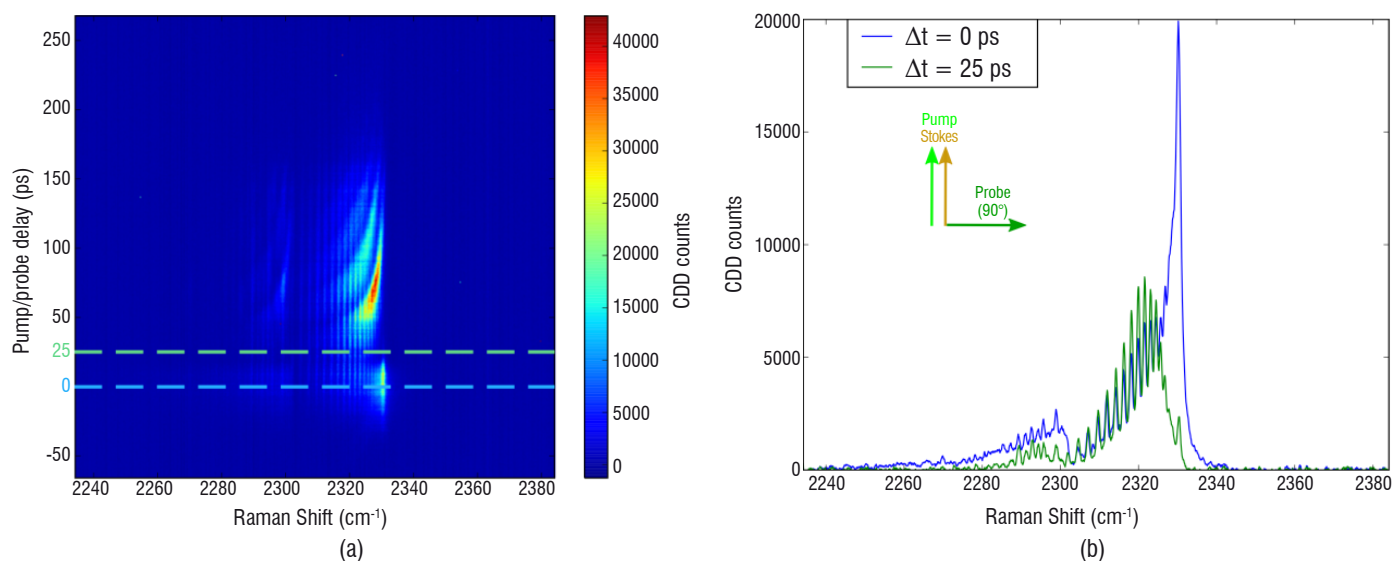


Figure 14 – N_2 CARS spectra recorded with vertical pump and Stokes, and horizontal probe polarizations. (a) Evolution of the spectrum (horizontal axis) with the probe delay (vertical axis). The two dashed lines indicate the 0 and 25 ps delays. (b) Spectra recorded at the 0 and 25 ps probe delay.

$\omega = \omega_{pump} - \omega_{Stokes}$, by convolving two terms: the molecular excitation, $A_{excitation}(\omega, \tau)$, which takes into account the pump/probe delay τ , and the probe spectrum $A_{probe}(\omega)$. The CARS intensity is thus given by:

$$I_{CARS}(\omega, \tau) = |A_{excitation}(\omega, \tau) \otimes A_{probe}(\omega)|^2 \quad (2)$$

Modeling of the molecular excitation

The molecular excitation $A_{excitation}(\omega, \tau)$ is expressed as the nonlinear susceptibility $\chi^{(3)}(\omega)$, weighted by the effective spectral profile $H(\omega)$ of the pump/Stokes excitation, and dephased by a term $\phi(\omega, \tau)$ that takes into account the free evolution of the coherences during the pump/probe delay τ :

$$A_{excitation}(\omega, \tau) = H(\omega) \chi^{(3)}(\omega) \phi(\omega, \tau) \quad (3)$$

The third order susceptibility $\chi^{(3)}(\omega)$ is composed of resonant and nonresonant contributions. The resonant amplitude depends on the pump, Stokes and probe polarizations, on the temperature, and the number density [1] [43]. Raman cross-sections, together with Doppler and collisional line broadening, are needed to properly simulate the profile. The resonant CARS susceptibility $\chi_R^{(3)}(\omega)$ is a sum of the nearby Raman lines expressed by [43]:

$$\chi_R^{(3)}(\omega) = \sum_{\alpha\beta} \left(\frac{d\sigma_{\alpha\beta}}{d\Omega} \right) \cdot \Delta\rho_{\alpha\beta} \cdot \frac{i\sqrt{\pi}}{\sqrt{2}\sigma_{Doppler}} \cdot W \left(\frac{\omega_{\alpha\beta} - \omega - i\Gamma_{\alpha\beta}}{\sqrt{2}\sigma_{Doppler}} \right), \quad (4)$$

where:

- $|\alpha\rangle$ and $|\beta\rangle$ are two ro-vibrational levels coupled by a Raman allowed transition,

- $\left(\frac{d\sigma_{\alpha\beta}}{d\Omega} \right)$ is the spontaneous Raman cross-section of the $|\alpha\rangle \rightarrow |\beta\rangle$ transition,

- $\omega_{\alpha\beta}$ is the Raman shift of the $|\alpha\rangle \rightarrow |\beta\rangle$ transition,

- $\Delta\rho_{\alpha\beta}$ is the population difference between the $|\alpha\rangle$ and $|\beta\rangle$ levels, which is a function of temperature (Boltzmann distribution),

- $\Gamma_{\alpha\beta}$ stands for the collisional broadening of the $|\alpha\rangle \rightarrow |\beta\rangle$ transition, the linewidths $\Gamma_{\alpha\beta}$ were taken from a fit of N_2 lines with an energy gap law standing for collisional effects including motional narrowing [44],

- $\sigma_{Doppler}$ is the Doppler broadening,

- $W(a + ib) = \frac{i}{\pi} \int_{-\infty}^{+\infty} \frac{e^{-t^2}}{a - t + ib} dt$ is the complex error function, giving

the spectral profile of each transition [43] considered as a complex Voigt profile resulting from Doppler and collisional effects.

Apart from the resonant CARS signal, a nonresonant background is generated, which is modeled as a constant scalar $\chi_{NR}^{(3)}$, potentially complex [37]. The whole susceptibility $\chi^{(3)}(\omega)$ is thus obtained by:

$$\chi^{(3)}(\omega) = \chi_R^{(3)}(\omega) + \chi_{NR}^{(3)} \quad (5)$$

The excitation amplitude profile $H(\omega)$ is introduced to take into account the finite excitation bandwidth of the pump and Stokes pulses.

It has been modeled by a real profile, since the dephasing between the different spectral parts, which can be nonzero due to the chirp of the pump pulse, is assumed to be negligible in our case. Indeed, the 2D plot in Figure 8 shows that all Raman lines are located at the same delay $\tau = 0$ along the abscissa, thus proving that coherences are not delayed significantly with respect to each other. Indeed, the excitation time window is limited to ~ 150 fs by the short duration of the Stokes pulse. In comparison, the smallest temporal modulation period observed in the Raman lines, estimated to be of about 20 ps in Figure 8, is thus two orders of magnitude larger than the excitation window.

In Figure 15, two different experimental conditions are shown. The pump/Stokes excitation profiles are shifted by 40 cm^{-1} to outline the effect on the CARS spectrum. Experimentally, excitation profiles are obtained by recording the CARS signal in Ar and by adjusting the temporal shift of the pump, thus providing $|H(\omega)|^2$.

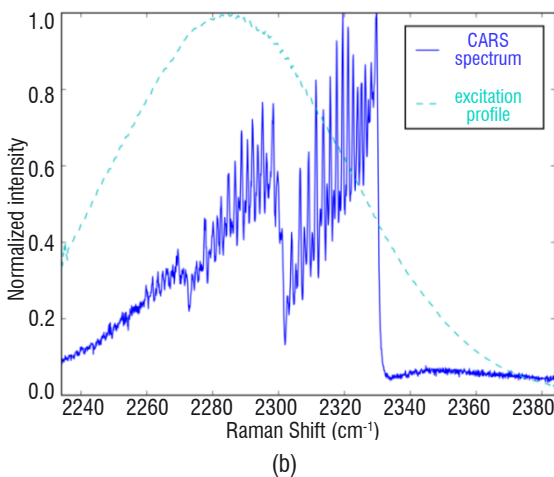
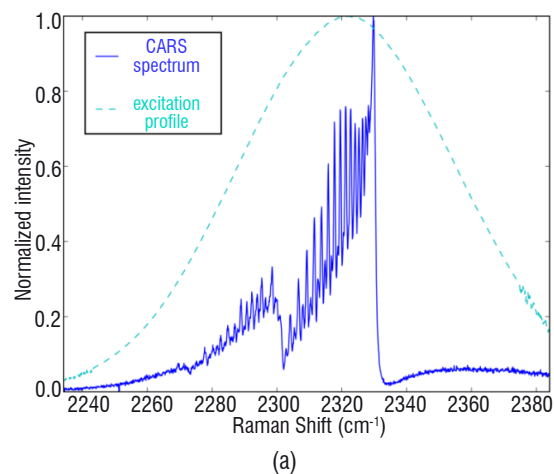


Figure 15 – CARS experimental spectra (blue) acquired over 5000 shots in a premixed CH_4 /air flame, with pump/Stokes excitation profiles $|H(\omega)|^2$ (dashed line) centered at (a) 2320 cm^{-1} and (b) 2280 cm^{-1} .

The dephasing term $\phi(\omega, \tau)$ is used to model the free evolution of the coherences during the time delay τ separating the excitation and the probing. It is expressed by:

$$\phi(\omega, \tau) = e^{i\omega\tau} \quad (6)$$

Finally, the complete molecular excitation is expressed by:

$$A_{excitation}(\omega, \tau) = H(\omega) \chi(\omega) e^{i\omega\tau} \quad (7)$$

Modeling of the probing step

During this step, the probe spectral pattern $A_{probe}(\omega)$ is convoluted to the molecular excitation $A_{excitation}(\omega, \tau)$, in order to produce the CARS spectrum. The final resolution is thus driven by the spectral width of the probe. In the temporal domain simulation, the crucial parameter is shown to be the pulse duration. The latter corresponds to the temporal window in which the molecular response is probed [37]. Finally, the CARS intensity can be expressed as follows:

$$I_{CARS}(\omega) = |H(\omega)\chi(\omega)e^{i\omega\tau} \otimes A_{probe}(\omega)|^2 \quad (8)$$

Since the probe spectral pattern is much narrower than the excitation profile, the factor $H(\omega)$ can be extracted from the convolution product and the calculation is implemented as follows:

$$I_{CARS}(\omega) = |H(\omega)|^2 \cdot |\chi(\omega)e^{i\omega\tau} \otimes A_{probe}(\omega)|^2 \quad (9)$$

The probe spectrum $A_{probe}(\omega)$ is measured (Figure 4 (a), thin solid line) and adjusted to fit a Voigt profile. However, a proper approach may be to consider the full complex amplitude of the probe spectrum, which can be obtained by recording the spectral shape with a spectrometer, and/or a combination of interferometric techniques such as FROG [45]. The excitation profile $|H(\omega)|^2$ is obtained by measuring the nonresonant response in Ar, as detailed previously. An overall view of the algorithm, including the convolution by apparatus function of the spectrometer, is summed up in Figure 16.

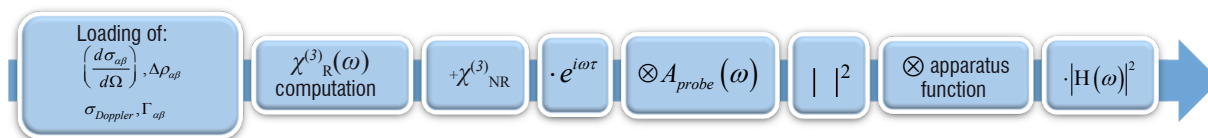
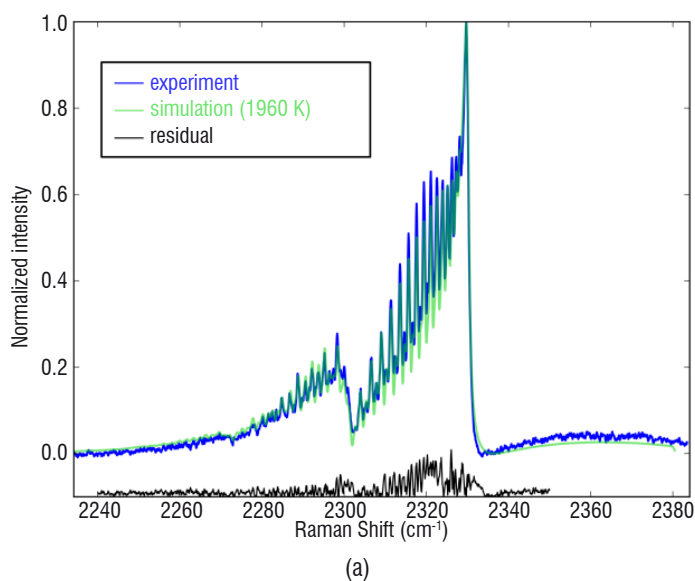


Figure 16 – Schematic view of the hybrid fs/ps-CARS simulation algorithm



Temperature measurements

The temperature is measured by comparing the experimental spectrum to a set of simulated spectra. A least-square algorithm, run over a bank of spectra, simulated by varying the temperature in 10 K steps and normalized to the unit maximum, leads to the best fit. The free parameter of the fit is thus the temperature, whereas the pump/probe delay and the nonresonant background amplitude are fixed. The least-square minimization range is chosen between 2250 cm⁻¹ (lowest line of $\nu=2$ band) and 2350 cm⁻¹, which provides information on both the R and NR contributions, as illustrated in Figure 5. In particular, it enables the choice of the fixed NR amplitude to be validated *a posteriori*.

The accuracy of the thermometric setup has been tested on two sets of experimental data at zero probe delay. The first set is a stack of 1000 single shots spectra, acquired at a repetition rate of 1 kHz in ambient air. The second one is composed of 100 spectra recorded in a premixed-CH₄/air flame with equivalent ratio $\phi = 1.0$ at atmospheric pressure. Each hot spectra is averaged over 500 shots, in order to reach a signal-to-noise ratio (SNR) beyond 120. The criticality of the SNR in hybrid fs/ps-CARS has been recently investigated by Kearney [46]. The probe delay parameter has been respectively fixed to 5.5 ps and 1.5 ps for the first and the second set, due to a small variation in the optical paths during the laser beam alignment.

Figure 17 and Figure 18 show a typical experimental spectrum (blue) superposed to its best fit (green). Temperature histograms, represented in Fig. 17 (b) and Fig. 18 (b), have been processed and were used to quantify the mean temperature $\langle T \rangle$, standard deviation σ_T , and relative precision defined by the $\sigma_T/\langle T \rangle$ ratio, which quantifies

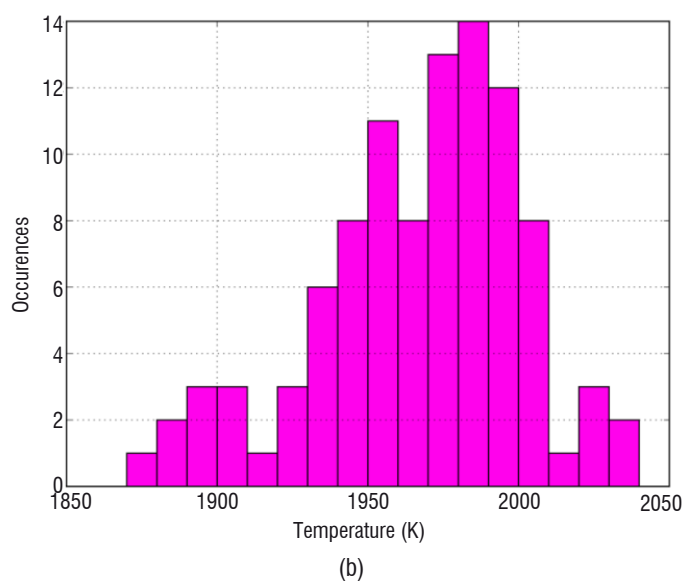


Figure 17 – CARS thermometry in a CH₄/air flame. (a) Typical experimental spectrum (blue), average best fit (green), and residual contribution (black) downshifted by 0.1 along the vertical axis. (b) Temperature histogram: $\langle T \rangle = 1960$ K, $\sigma_T = 35$ K

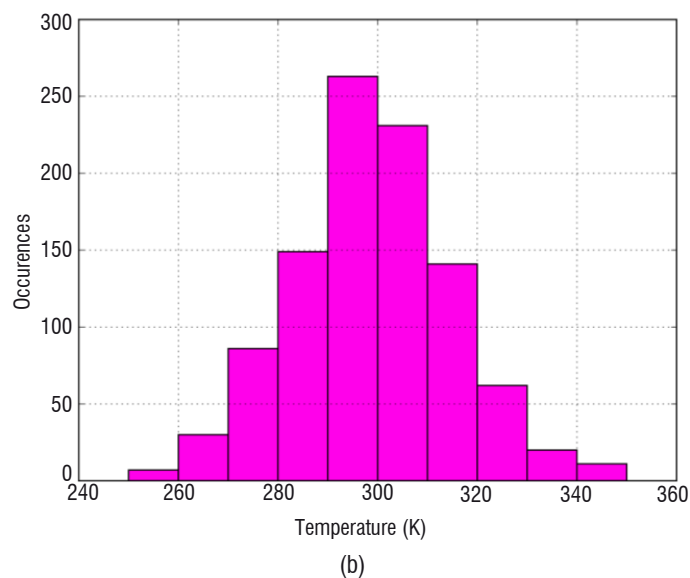
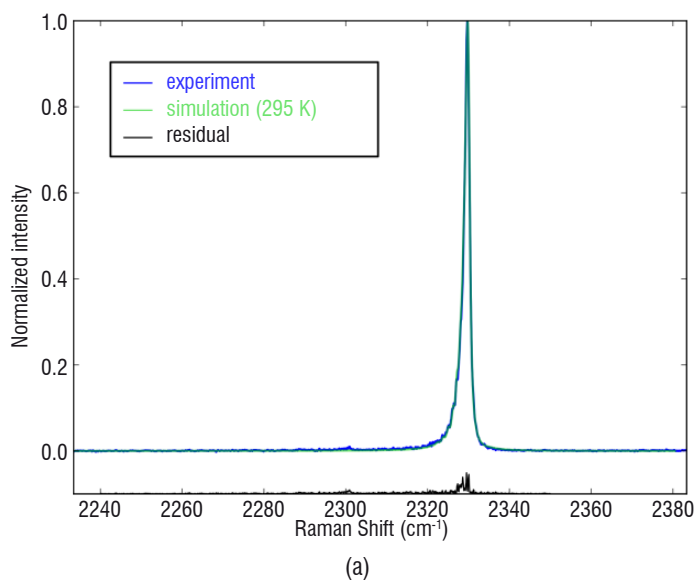


Figure 18 – CARS thermometry in ambient air. (a) Typical experimental spectrum (blue), average best fit (green), and residual contribution (black) downshifted by 0.1 along the vertical axis. (b) Temperature histogram: $\langle T \rangle = 295$ K, $\sigma_T = 15$ K

the repeatability of the measurement. In ambient air and in the flame, the estimated mean temperatures were respectively 295 and 1960 K, with corresponding precisions of 5.2% (15 K) and 1.7% (35 K). The temperature in the flame was measured to be slightly lower than the adiabatic CH_4/air flame temperature (~ 2200 K). This was attributed to experimental misalignment of the probed volume in the flame, and to nonzero pump/probe delay adjustment. This measurement will be reproduced in a better controlled flame and using a well-calibrated procedure to accurately and rapidly control the pump/probe delay. It is comparable to the few percent precision obtained with hybrid fs/ps rotational CARS [46], fs-CPP-CARS [47], and ns-CARS [48] in a flame. To go further in the characterization of the techniques, single shot thermometry at low and high temperatures would be of great significance, in order to avoid integrating spectra over the flame temperature fluctuations. This new process in our setup development would require a more energetic probe, whose small bandwidth is currently achieved at the expense of an important loss of energy, due to the filtering technique used. Using nonlinear techniques [32], so as to achieve more efficient narrowing, would be one way to achieve this goal.

Perspectives and conclusion

In summary, hybrid fs/ps-CARS was used to properly resolve ro-vibrational structures of the Q-branch of N_2 . The resolution was good enough to observe both rotational and vibrational features in a single spectrum, as had already been done in ns-CARS, thus opening the way to instantaneous rotational and vibrational temperature measurements. Moreover, time domain spectroscopy was used, in order to resolve sub-probe bandwidth details in the spectrum.

Temperature measurements were performed in the flame, by comparing simulations to experiments, with good accuracy. The model will be improved by taking into account non-diagonal elements of the relaxation matrix, i.e., motional narrowing effects. The calculation of motional narrowing in hybrid fs/ps-CARS is under study, in order to achieve our final objective, which is to probe both high pressure and high temperature media. The long probe duration that is required for spectral resolution will be further combined to an increase in the energy of the probe, to achieve single shot measurements ■

Acknowledgments:

Frederic Grisch is greatly thanked for his constant support and advice regarding both the experiments and the simulations. We also thank Hans Stauffer and Sean Kearney, who helped us to clarify important theoretical aspects through fruitful discussions. We are grateful to Jean Pierre Faleni and Thomas Schmid for their technical assistance with the burner design and gas supply. Funding was provided by the SESAME program of the *Conseil Régional d'Ile de France* (13016393), thanks to which part of the equipment was obtained.

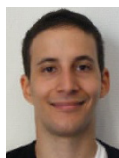
References

- [1] S.A.J. DRUET and J.-PE. TARAN - *CARS Spectroscopy*. Prog.Quant. Electronics, vol. 7, p. 1, 1981.
- [2] S.A.J. DRUET, B. ATTAL, T.K. GUSTAFSON and J.P. TARAN - *Electronic Resonance Enhancement of Coherent Anti-Stokes Raman Scattering*. Physical Review A, vol. 18, no. 4, p. 1529, 1978.
- [3] BLOEMBERGEN - *Nonlinear Optics*. 31977th ed.: WA Benjamin New York, 1965.
- [4] A.C. ECKBRETH - *Laser Diagnostics for Combustion Temperature and Species*. 2nd ed. Amsterdam: Gordon and Breach Publishers, 1996.
- [5] P.D. MAKER and R.W. TERHUNE - *Study of Optical Effects Due to an Induced Polarization Third Order in the Electric Field Strength*. Phys. Rev, vol. 137, no. 3A, p. A801, 1965.
- [6] P.R. REGNIER and J.P.-E. TARAN - *On the Possibility of Measuring Gas Concentrations by Stimulated Anti-Stokes Scattering*. Applied Physics Letters, vol. 23, p. 240, 1973.
- [7] W.B. ROH, P.W. SCHREIBER and J.P.-E. TARAN - *Single-Pulse Coherent Anti-Stokes Raman Scattering*. Single-pulse Coherent anti-Stokes Raman Scattering, vol. 29, no. 3, p. 174, 1976.
- [8] S. ROY, P.S. HSU, N. JIANG, M.N. SLIPCHENKO and J.R. GORD - *100-kHz-Rate Gas-Phase Thermometry Using 100-Ps Pulse from a Burst-Mode Laser*. Optics Letters, vol. 40, no. 21, p. 5125, 2015.
- [9] S. ROY, W.D. KULATILAKA, D.R. RICHARDSON, R.P. LUCHT and J.R. GORD - *Gas-Phase Single-Shot Thermometry at 1 kHz Using Fs-CARS Spectroscopy*. Optics Letters, vol. 34, no. 24, p. 2857, 2009.
- [10] C.C. HAYDEN and D.W. CHANDLER - *Femtosecond Time-Resolved Studies of Coherent Vibrational Raman Scattering in Large Gas-Phase Molecules..* The Journal of Chemical Physics, vol. 103, no. 24, p. 10465, 1995.
- [11] P. BEAUD, H.-M. FREY, T. LANG and M. MOTZKUS - *Flame Thermometry by Femtosecond CARS*. Chemical Physics Letters, vol. 344, p. 407, 2001.
- [12] B. LAVOREL, H. TRAN, E. HERTZ, O. FAUCHER, P. JOUBERT, M. MOTZKUS, T. BUCKUP, T. LANG, H. SKENDEROVI, G. KNOPP, P. BEAUD and H.M. FREY - *Femtosecond Raman Time-Resolved Molecular Spectroscopy*. Comptes Rendus Physique, vol. 5, p. 215, 2004.
- [13] S. ROY, T. MEYER and J.R. GORD - *Broadband Coherent Anti-Stokes Raman Scattering Spectroscopy of Nitrogen Using a Picosecond Modeless Dye Laser*. Optics Letters, vol. 30, no. 23, p. 3222, 2005.
- [14] W. ZINTH - *Transient Coherent Raman Scattering in the Time and Frequency Domain*. Optics Communications, vol. 34, no. 3, p. 479, 1980.
- [15] B.D. PRINCE, A. CHAKRABORTY, B.M. PRINCE, and H.U. STAUFFER - *Development of Simultaneous Frequency- and Time-Resolved Coherent Anti-Stokes Raman Scattering for Ultrafast Detection of Molecular Raman Spectra*. The Journal of Chemical Physics, vol. 125, p. 044502, 2006.
- [16] J.D. MILLER, S. ROY, M.N. SLIPCHENKO, J.R. GORD, and T.R. MEYER - *Single-Shot Gas-Phase Thermometry Using Pure-Rotational Hybrid Femtosecond-Picosecond Coherent Anti-Stokes Raman Scattering*. Optics Express, vol. 19, no. 16, p. 15627, 2011.
- [17] J.D. MILLER, M.N. SLIPCHENKO, T.R. MEYER, H.U. STAUFFER, and J.R. GORD - *Hybrid Femtosecond/Picosecond Coherent Anti-Stokes Raman Scattering for High-Speed Gas-Phase Thermometry*. Optics Express, vol. 35, no. 14, p. 2430, 2010.
- [18] A. BOHLIN and C.J. KLIEWER - *Two-Beam Ultrabroadband Coherent Anti-Stokes Raman Spectroscopy for High Resolution Gas-Phase Multiplex Imaging*. Applied Physics Letters, vol. 104, p. 031107, 2014.
- [19] A. BOHLIN and C.J. KLIEWER - *Communication: Two-Dimensional Gas-Phase Coherent Anti-Stokes Raman Spectroscopy (2D-CARS): Simultaneous Planar Imaging and Multiplex Spectroscopy in a Single Laser Shot*. The Journal of Chemical Physics, vol. 138, p. 221101, 2013.
- [20] D. MESSINA, B. ATTAL-TRETOUT and F. GRISCH - *Study of a Non-Equilibrium Pulsed Nanosecond Discharge at Atmospheric Pressure Using Coherent Anti-Stokes Raman Scattering*. Proceedings of the Combustion Institute, vol. 31, no. 1, p. 825, 2007.
- [21] W. ZINTH, A. LAUBEREAU and W. KAISER - *Time Resolved Observation of Resonant and Non-Resonant Contributions to the Nonlinear Susceptibility*. Optics Communications, vol. 26, no. 3, p. 457, 1978.
- [22] F.M. KAMGA and M.G. SCEATS - *Pulse-Sequenced Coherent Anti-Stokes Raman Scattering Spectroscopy: A Method for Suppression of the Nonresonant Background*. Optics Letters, vol. 5, no. 3, p. 126, 1980.
- [23] J.D. MILLER, C.E. DEDIC and T.E. MEYER - *Vibrational Femtosecond/Picosecond Coherent Anti-Stokes Raman Scattering with Enhanced Temperature Sensitivity for Flame Thermometry from 300 to 2400 K*. Journal of Raman Spectroscopy, vol. 46, p. 702, 2015.
- [24] M. SCHERMAN, M. NAFA, T. SCHMID, A. GODARD, A. BRESSON, B. ATTAL-TRETOUT and P. JOUBERT - *Rovibrational Hybrid fs/ps CARS Using a Volume Bragg Grating for N₂ Thermometry*. Optics Letters, vol. 41, no. 3, p. 488, 2016.
- [25] A.C. ECKBRETH - *BOXCARS: Crossed-Beam Phase-Matched CARS Generation in Gases*. Applied Physics letters, vol. 32, p. 421, 1978.
- [26] D. ORON, N. DUDOVICH, D. YELIN AND Y. SILBERBERG - *Narrow-Band Coherent Anti-Stokes Raman Signals from Broad-Band Pulses*. Physical Review Letters, vol. 88, no. 6, p. 063004, 2002.
- [27] S. ROY, P. WRZESINSKI, D. PESTOV, T. GUNARATNE, M. DANTUS and J.R. GORD - *Single-Beam Coherent Anti-Stokes Raman Scattering Spectroscopy of N₂ Using a Shaped 7 Fs Laser Pulse*. Applied Physics Letters, vol. 95, p. 074102, 2009.
- [28] S.O. KONOROV, M.W. BLADES and R.F.B. TURNER - *Lorentzian Amplitude and Phase Pulse Shaping for Nonresonant Background Suppression and Enhanced Spectral Resolution in Coherent Anti-Stokes Raman Scattering Spectroscopy and Microscopy*. Applied Spectroscopy, vol. 64, no. 7, p. 767, 2010.

- [29] O. KATZ, J.M. LEVITT, E. GRINVALD and Y. SILBERBERG - *Single-Beam Coherent Raman Spectroscopy and Microscopy via Spectral Notch Shaping*. Optics Express, vol. 18, no. 22, p. 22693, 2010.
- [30] V. KUMAR, R. OSELLAME, R. RAMPONI, G. CERULLO and M. MARANGONI - *Background-Free Broadband CARS Spectroscopy from a 1-MHz Ytterbium Laser*. Optics Express, vol. 19, no. 16, p. 15143, 2011.
- [31] S.P. KEARNEY, D.J. SCOGLIETTI and C.J. KLIEWER - *Hybrid Femtosecond/Picosecond Rotational Coherent Anti-Stokes Raman Scattering Temperature and Concentration Measurements Using Two Different Picosecond-Duration Probes*. Optics Express, vol. 21, no. 10, p. 12327, 2013.
- [32] S.P. KEARNEY and D.J. SCOGLIETTI - *Hybrid Femtosecond/Picosecond Rotational Coherent Anti-Stokes Raman Scattering at Flame Temperatures Using a Second-Harmonic Bandwidth-Compressed Probe*. Optics Letters, vol. 38, no. 6, p. 833, 2013.
- [33] J.D. MILLER, M.N. SLIPCHENKO and T.R. MEYER - *Probe-Pulse Optimization for Nonresonant Suppression in Hybrid fs/ps Coherent Anti-Stokes Raman Scattering at High Temperature*. Optics Express, vol. 19, no. 4, p. 13326, 2011.
- [34] H.U. STAUFFER, J.D. MILLER, S. ROY, J.R. GORD and T.R. MEYER - *Hybrid Femtosecond/Picosecond Rotational Coherent Anti-Stokes Raman Scattering Thermometry Using a Narrowband Time-Asymmetric Probe Pulse*. The Journal of Chemical Physics, vol. 136, no. 11, p. 111101, 2012.
- [35] J. LUMEAU, V. SMIRNOV, A. GLEBOV and L.B. GLEBOV - *Ultra-Narrow Bandpass Filters Based on Volume Bragg Grating Technologies*. Proc. of SPIE, vol. 7675, p. 76750H, 2010.
- [36] HERZBERG - *Molecular Spectra and Molecular Structure. I. Spectra of Diatomic Molecules.*: Van Nostrand, 1950.
- [37] H.U. STAUFFER, J.D. MILLER, M.N. SLIPCHENKO, T.R. MEYER, B.D. PRINCE, S. ROY and J.R. GORD - *Time- and Frequency-Dependent Model of Time-Resolved Coherent Anti-Stokes Raman Scattering (CARS) with a Picosecond-Duration Probe Pulse*. The Journal of Chemical Physics, vol. 140, p. 024316, 2014.
- [38] C.E. DEDIC, J.D. MILLER and T.R. MEYER - *Dual-Pump Vibrational/Rotational Femtosecond/Picosecond Coherent Anti-Stokes Raman Scattering Temperature and Species Measurements*. Optics Letters, vol. 39, no. 23, p. 6608, 2014.
- [39] D. ORON, N. DUDOVITCH and Y. SILBERBERG - *Femtosecond Phase-and-Polarization Control for Background-Free Coherent Anti-Stokes Raman Spectroscopy*. Physics Review Letters, vol. 90, no. 21, p. 213902, 2003.
- [40] A.F. BUNKIN, S.G. IVANOV and N.I. KOROTEEV - *Soviet Technical Physics Letters*. vol. 3, p. 182, 1977.
- [41] L.A. RAHN, L.J. ZYCH and P.L. MATTERN - *Background Free CARS Studies of Carbon Monoxide in a Flame*. Optics Communications, vol. 30, no. 2, p. 249, 1979.
- [42] F. VESTIN, M. AFZELIUS and P-E. BENGTSSON - *Development of Rotational CARS for Combustion Diagnostics Using a Polarization Approach*. Proceedings of the Combustion Institute, vol. 31, no. 1, p. 833, 2007.
- [43] F. EL-DIASTY - *Coherent Anti-Stokes Raman Scattering: Spectroscopy and Microscopy*. Vibrational Spectroscopy, vol. 55, no. 1, p. 1, 2011.
- [44] M. DHYNE, M. LEPERE, and P. JOUBERT - *Semiclassical Line Broadening Calculations, Using an Ab Initio Potential Energy Surface, in Q-Branch and S-Branch of N₂ Perturbed by H₂*. Journal of Raman Spectroscopy, vol. 43, p. 2008, 2012.
- [45] C. DORRER and M. JOFFRE, *Characterization of the Spectral Phase of Ultrashort Light Pulses*. Comptes-rendu de l'Académie des Sciences de Paris, p. 1415, 2001.
- [46] S.P. KEARNEY - *Hybrid fs/ps Rotational CARS Temperature and Oxygen Measurements in the Product Gases of Canonical Flat Flames*. Combustion and Flame, vol. 162, no. 5, p. 1748, 2015.
- [47] D.R. RICHARDSON, R.P. LUCHT, W. D. KULATILAKA, S. ROY and J.R. GORD - *Theoretical Modeling of Single-Laser-Shot, Chirped-Probe-Pulse Femtosecond Coherent Anti-Stokes Raman Scattering Thermometry*. Applied Physics B, vol. 104, no. 3, p. 699, 2011.
- [48] T. SEEGER and A. LEIPERTZ - *Experimental Comparison of Single-Shot Broadband Vibrational and Dual-Broadband Pure Rotational Coherent Anti-Stokes Raman Scattering in Hot Air*. Applied Optics, vol. 35, no. 15, p. 2665, 1996.

Acronyms

CARS	(Coherent Anti-Stokes Raman Scattering)
FPE	(Fabry Perot Etalon)
OPA	(Optical Parametric Amplifier)
NR	(Nonresonant)
R	(Resonant)
VBG	(Volume Bragg Grating)



Malik Nafa, graduated from the *Institut d'Optique* Graduate School in 2014. He is now a PhD student at ONERA working on the hybrid fs/ps CARS setup and on the simulation model described in this paper for thermometry applications in reactive flows.



Michael Scherman received his PhD in 2012 from *Université Pierre et Marie Curie*. He has been a research scientist at ONERA since then, in charge of the development of coherent and spontaneous Raman techniques applied to diagnostics in gaseous reactive flows, material characterization and biological sample studies.



Alexandre Bresson, received his Ph.D. degree in 2000, for his work on “quantitative imaging based on a laser-induced fluorescence technique” at ONERA – the French aerospace lab. He has been working for 4 years at ONERA, specifically on the development of optical diagnostic tools for combustion. Since 2004, he has continued his research on the use of cold atoms for on-board inertial sensing. He currently leads the “laser source and metrology” research unit at ONERA, in Palaiseau.



Alexandre Aubin is a student from the *Institut Universitaire de Technologie d'Orsay*. He built a stabilized CH₄/air flame, which is used in the lab as a reference of temperature for the CARS experiments.



Antoine Godard received his PhD from the *Laboratoire Charles Fabry de l'Institut d'Optique* in 2003. His research interests at ONERA concern the development of innovative laser sources based on nonlinear optics and their applications (gas sensing, onboard applications, etc.).



Brigitte Attal-Trétout performed the first Coherent Anti-Stokes Raman Scattering spectroscopy (CARS) experiments at ONERA. The so-called “resonant” version of CARS was created within this framework and used to record the first spectra of iodine. Since then, the Raman techniques and their degenerated version have been very widely applied to the measurement of traces in reactive environments. Brigitte Attal-Trétout has worked on optical metrology and nonlinear spectroscopy applied to plasmas and flames. She has directed a research unit and oriented field of applications to nano-object detection during their synthesis together with atom concentration measurements during material synthesis and in propellants flames. Finally, she constructed a CARS microscope for biology. Brigitte Attal-Trétout is currently a research director and scientific deputy of the Department of instrumentation and sensing.



Pierre Joubert works on the topic of molecular spectroscopy. He has performed semi-classical calculations of line broadening and line shifting coefficients applied to molecular systems involved in combustion media. He has also developed new spectral line profile models implemented using various thermometry techniques for a wide range of pressures and temperatures. He is the head of a physics and astrophysics research group at the UTINAM Institute. Pierre Joubert is currently a professor at Franche-Comté University.